Wiley Online Library
Early View publication on www.wileyonlinelibrary.com
(issue and page numbers not yet assigned;
citable using Digital Object Identifier – DOI)

Phys. Status Solidi B, 1–7 (2015) / DOI 10.1002/pssb.201451410

physica status solidi b
www.pss-b.com
basic solid state physics

Electron transmission through step-like potential in armchair and zigzag graphene nanoribbons: Comparison of different interfaces

Alexander Onipko and Lyuba Malysheva*

Bogolyubov Institute for Theoretical Physics, 03680 Kiev, Ukraine

Received 7 August 2014, revised 6 April 2015, accepted 7 April 2015
Published online 5 May 2015

Keywords electron transmission, graphene, interfaces, nanoribbons, step-like potential, tight-binding Hamiltonian

* Corresponding author: e-mail malysh@bitp.kiev.ua, Phone: +380 44 5213149, Fax: +380 44 5265998

We present the one-electron spectrum and eigenstates of bounded graphene nanoribbons that describe electron dynamics in terms of transverse and longitudinal motion. On this basis, we find the transmission coefficients for armchair graphene nanoribbons and polyacene under step-like electronic potential. The problem is solved for different interfaces between the regions with zero and nonzero site energies. The obtained results have numerous applications to the construction of multi-terminal graphene-based electronic devices.

1 Introduction The fascinating properties of graphene, an atom-thick layer of carbon atoms arranged in a honeycomb lattice, are documented in many experiments [1–5]. The unique combination of electronic properties and a comparative easiness of its fabrications shows that graphene is a candidate number one for a variety of applications, including future electronics and sensing.

In recent years, the electron behavior in graphene has been extensively studied by various methods of analytic and numerical modeling. Graphene ribbons (GRs) with armchair- and zigzag-shaped edges are most frequent objects of the investigation with the help of either Dirac equation [6–9] or Schrödinger equation with tight-binding Hamiltonian [10–16]. In the present study, we use the latter approach.

The honeycomb graphene lattice suggests six equivalent armchair- and six equivalent zigzag shaped electron pathways alternating every 30°. In Fig. 1a, these pathways are indicated by the chains of polyperylene and polyacene. A sheet of graphene with mutually perpendicular armchair and zigzag edges can be regarded as a pile of $\mathcal{N}$ in-plane stacked N-long parachained phenylenes or, alternatively, as N covalently bonded $\mathcal{N}$-long acenes. It is obvious that making N or $\mathcal{N}$ infinite, we obtain basic graphene structures: an armchair graphene ribbon (aGR, Fig. 1b) or a zigzag graphene ribbon (zGR, Fig. 1c). Proceeding further, we can make the aGR (or zGR) width infinitely large, which gives us an infinite sheet of graphene. The solution of the eigenvalue problem for aGR and zGR is thus crucial for understanding the dispersion and transmission in graphene in 12 different directions.

For many practical applications, a very important problem is the particle transmission under a potential with step-like profile. In this study, we consider electron transmission through graphene ribbons with site energies taking the values 0 and U, as shown in Fig. 1b–d. Unlike previous works [17–19], we perform calculations of the through-step transmission coefficient for different interfaces between the regions with zero and nonzero site energies. We emphasize that the proposed approach allows us to consider different interfaces, in contrast to the continuous model of Dirac fermions. It is shown that the difference between the dependences of the transmission coefficients for different types of interfaces is well pronounced and, presumably, can be evaluated in the course of the experimental investigations.

The transmission coefficients are found for two types of GRs: with armchair and zigzag boundaries. The armchair nanoribbons are considered for any width $\mathcal{N}$ with a special emphasis on polyperylene, i.e., on an aGR of width $\mathcal{N}=2$ (2aGR). For the zigzag nanoribbons, the mathematical approach is much more complicated. To the best of our knowledge, the problem of finding the explicit expressions for the

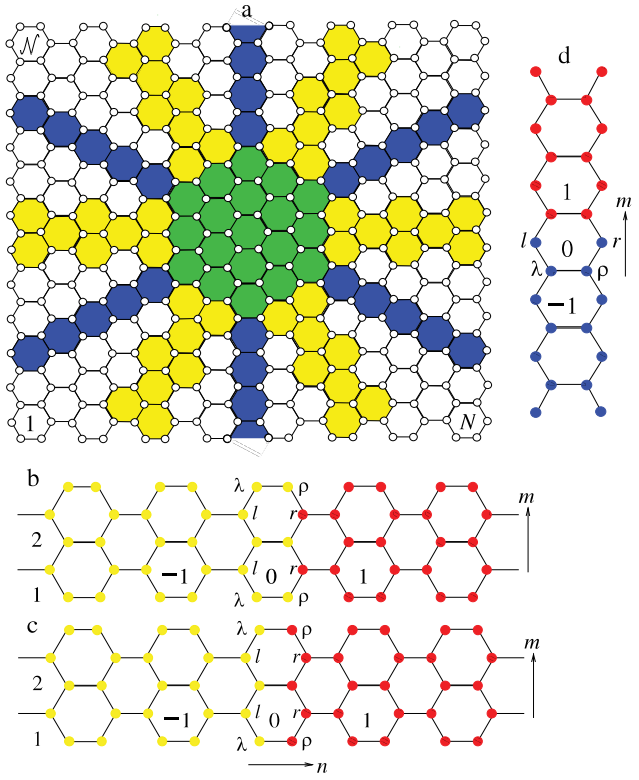

Figure 1 (a) $N\times\mathcal{N}$ sheet of graphene. The sixfold local symmetry of an infinite honeycomb lattice is highlighted by the segments of polyperylene (yellow) and polyacene (blue). (b and c) Structure of polyperylene, which is also referred in the text as 2aGR. The yellow and red circles indicate zero and U-shifted site energies of carbon atoms modeling ρ–r and λ–ρ interfaces of the potential step U. (d) Polyacene chain which is also abbreviated in the text as 1zGR. The change in the color of circles from blue to red corresponds to the l–λ potential step. Location of carbon atoms is specified by the numbers m, n, and the label $\alpha = l, \lambda, \rho, l$. Hydrogen atoms along the edges of graphene sheet, polyperylene, and polyacene are not shown.

transmission coefficient in the zigzag nanoribbons was not discussed in the literature. Thus, we restrict ourselves to the case of polyacene, a zGR with the width $N = 1$ (1zGR) illustrating several principal properties exhibited by graphene in the zigzag direction. It should be stressed that the narrow ribbons 2aGR and 1zGR are of considerable interest themselves because they are potentially useful for different multiterminal graphene-based electronic devices, as shown in Fig. 1a.

2 Transmission in aGR In the nearest-neighbor approximation, for the lattice site enumeration explained in Fig. 1, the tight-binding Hamiltonian of aGR can be represented as

$$H = \sum_{\mathbf{r}'-\mathbf{r}=\mathbf{q}} \sum_{\mathbf{r}} [\varepsilon_{\mathbf{r}}(1-\delta_{\mathbf{q},\mathbf{0}}) - \beta] b^{+}_{\mathbf{r}} b_{\mathbf{r}+\mathbf{q}}, \tag{1}$$

where $b^{+}_{\mathbf{r}}$ ($b_{\mathbf{r}}$) is the electron creation (annihilation) operator at $\mathbf{r} = m, n, \alpha$; $\varepsilon_{\mathbf{r}}$ and $-\beta$ ($\beta > 0$) are, respectively, the electron site energy and hopping integral.

In this representation, the wave function of π electron reads $\Psi = \sum_{\mathbf{r}} \psi_{\mathbf{r}} b^{+}_{\mathbf{r}} |0\rangle$, where the expansion coefficients obey (for any n) the set of equations (energy is always expressed in the units of β)

$$\begin{aligned}
(E-\varepsilon_n)\underset{m=1,2,\ldots,\mathcal{N}}{\psi_{m,n,l}} &= -\psi_{m,n-1,r} - \psi_{m,n,\lambda} - \psi_{m+1,n,\lambda},\\
(E-\varepsilon_n)\underset{m=1,2,\ldots,\mathcal{N}+1}{\psi_{m,n,\lambda}} &= -\psi_{m,n,l} - \psi_{m-1,n,l} - \psi_{m,n,\rho},\\
(E-\varepsilon_n)\underset{m=1,2,\ldots,\mathcal{N}+1}{\psi_{m,n,\rho}} &= -\psi_{m,n,r} - \psi_{m-1,n,r} - \psi_{m,n,\lambda},\\
(E-\varepsilon_n)\underset{m=1,2,\ldots,\mathcal{N}}{\psi_{m,n,r}} &= -\psi_{m,n+1,l} - \psi_{m,n,\rho} - \psi_{m+1,n,\rho},\\
\psi_{0,n,l} = \psi_{0,n,r} &= \psi_{\mathcal{N}+1,n,l} = \psi_{\mathcal{N}+1,n,r} = 0.
\end{aligned} \tag{2}$$

For a potential step U located between the atoms in r and l positions, $\varepsilon_{n\le 0} = 0$ and $\varepsilon_{n\ge 1} = U$, the scattering-type solution to the equations presented above was found for an arbitrary width of aGR [17, 18]. Here, we will see that the solution is different for the location between the nearest-neighbor atoms in, e.g., the ρ and r (as in Fig. 1b), and λ and ρ positions (as in Fig. 1c). However, this difference is shown to manifest itself in the transmission coefficient only in the former case but not in the latter. In other words, the transmission through the potential step at the r–l and λ–ρ interfaces is identical but it is different when an electron meets the potential step at the ρ–r and l–λ interfaces. To our knowledge, the potential was supposed to change just between nearest-neighbor r and l atoms in all related studies [8, 17–19].

Labeling the wave function to the left and right of the interface by L and R, respectively, we can write the solution to Eq. (2) in a single-mode form

$$\begin{aligned}
\psi^{\mathrm{L}}_{m,n,\alpha} &= \psi^{(j)}_{m,n,\alpha}(k) + r^{(j)}\psi^{(j)\,*}_{m,n,\alpha}(k),\\
\psi^{\mathrm{R}}_{m,n,\alpha} &= t^{(j)}\psi^{(j)}_{m,n,\alpha}(\bar{k}),
\end{aligned} \tag{3}$$

where $\psi^{(j)}_{m,n,\alpha}$ ($j = 1, 2, \ldots, \mathcal{N}$) is an eigenstate of aGR. For the zero site energies, the corresponding dispersion relation takes the form [11]

$$E_j^2 = 1 + \mu_j^2 \pm 2\mu_j \cos(\sqrt{3}k/2), \quad \mu_j \equiv 2\cos(\xi_j/2), \tag{4}$$

where $\xi_j = \pi j/(\mathcal{N}+1)$, and the wave vector k, $0 \le k \le \pi$, is in the units of a^{-1}. The wave vector marked by the overbar ($\bar{k}$), as well as the corresponding eigenenergy $\bar{E}_j$, refer to the aGRs with site energies shifted by U: $\bar{E}_j = E_j - U$. The sign $\pm$ in Eq. (4) marks the "plus" and "minus" branches of the dependence $E_j(k)$. The mode with the lowest absolute energy belongs to the "minus" branch. Moreover, the energy E_{j^*}

($j^* = 2(\mathcal{N}+1)/3$) equals zero for metallic aGRs for which $(\mathcal{N}+1)/3$ is an integer number.

It is easy to see that, for any particular place of changes in the site energy, the substitution of Eq. (3) in Eq. (2) results in two equivalent pairs of equations for the unknown amplitudes of reflection $r^{(j)}$ and transmission $t^{(j)}$. It is clear that to find two quantities (reflection and transmission coefficients), we need only two equations from system (2). The reason to write four equations is that we want to find the transmission coefficients for different types of interfaces. Thus, for each type we use a corresponding pair of equations from system (2). Namely, for the ρ–r interface (Section 2.1), we use the third and fourth equations of Eq. (2), for the λ–ρ interface (Section 2.2) – the second and third equations, while for the r–l interface we use the first and fourth equations of system (2).

The eigenfunctions $\psi^{(j)}_{m,n,\alpha}(k)$ can be found by using different approaches [12, 14–16]. Here, it is convenient to use the phase representation

$$\psi^{(j)}_{m,n,\alpha} = \begin{cases} e^{i[\sqrt{3}k(n-1)+\theta]}\sin(\xi_j m), & \alpha = l, \\ \pm e^{i\sqrt{3}k(n-1/2)}\sin[\xi_j(m-1/2)], & \alpha = \lambda, \\ \pm e^{i[\sqrt{3}k(n-1/2)+\theta]}\sin[\xi_j(m-1/2)], & \alpha = \rho, \\ e^{i\sqrt{3}kn}\sin(\xi_j m), & \alpha = r, \end{cases} \tag{5}$$

where the phase θ is defined as follows:

$$e^{i\theta} = -\frac{1}{E_j}\left(1 \pm \mu_j e^{i\sqrt{3}k/2}\right), \qquad 0 \le \theta \le \pi. \tag{6}$$

The $\pm$ sign in Eqs. (5) and (6) corresponds to the "plus" and "minus" branches of Eq. (4). The phase factor was first introduced in Ref. [17], where the functions $\psi^{(j)}_{m,n,l}$, $\psi^{(j)}_{m,n,r}$ were represented in the form (5).

As follows from Eq. (5), the phase factor is determined by the phase difference between neighboring A, B sites represented by the pairs r–l and λ–ρ. It follows from Eq. (6) that

$$|E_j e^{i\theta} + 1|^2 = \mu_j^2. \tag{7}$$

We also see that, since E_j can be positive or negative, θ is a discontinuous function of energy. However, we can use instead a continuous variable $0 \le \theta \le \pi$, which implies that $\theta \Longrightarrow |\theta|$. Then, by analogy with Eq. (4), the above equation can be regarded as the phase dispersion relation. Similarly, for $U \neq 0$, we get $|\bar{E}_j e^{i\bar{\theta}} + 1|^2 = \mu_j^2$. Henceforth, the phases θ and $\bar{\theta}$ should be understood as explained.

Equations (1)–(6) suggest an instrumental framework for the evaluation of the through-step transmission coefficient for different interfaces between the regions with zero and nonzero site energies. It is free of the necessity of application of matching conditions whose choice is somewhat arbitrary. In addition, it is much easier than calculations with the use of Green's functions [18], which must be defined for semiinfinte aGRs with different terminations.

2.1 l–λ and ρ–r interfaces It is obvious from the system symmetry that the transmission coefficients for l–λ and ρ–r interfaces are identical. Their common feature is that the potential changes between the sites which belong to different parallel chains of A–B pairs, whereas the phase difference refers to A–B pairs within the same chain; see Eq. (5). To consider the potential step dividing ρ and r sites, we can use two out of four equations in Eq. (2). Specifically, instead of the last two equations for $n = 0$, we can write

$$\begin{aligned} E\psi^{\mathrm{L}}_{m,0,\rho} &= -\psi^{\mathrm{R}}_{m,0,r} - \psi^{\mathrm{R}}_{m-1,0,r} - \psi^{\mathrm{L}}_{m,0,\lambda}, \\ \bar{E}\psi^{\mathrm{R}}_{m,0,r} &= -\psi^{\mathrm{R}}_{m,1,l} - \psi^{\mathrm{L}}_{m,0,\rho} - \psi^{\mathrm{L}}_{m+1,0,\rho}, \end{aligned} \tag{8}$$

where $\psi^{\mathrm{L}}_{m,n,\alpha}$ and $\psi^{\mathrm{R}}_{m,n,\alpha}$ are defined in Eq. (3).

Finding $t^{(j)}$ with the use of Eqs. (5) and (8) is the matter of simple algebra. The substitution of the result into

$$\begin{aligned} T^{(j)} &= \frac{\bar{v}_j}{v_j}\left|t^{(j)}\right|^2 = \frac{\sin(\sqrt{3}\,\bar{k}/2)}{\sin(\sqrt{3}k/2)}\left|\frac{E_j}{\bar{E}_j}\right|\left|t^{(j)}\right|^2 \\ &= \frac{\sin\bar{\theta}}{\sin\theta}\left|t^{(j)}\right|^2 \end{aligned} \tag{9}$$

yields

$$T^{(j)}_{\alpha-\alpha'} = \frac{\sin\theta\sin\bar{\theta}}{\left|\sin^2[(\theta+\bar{\theta})/2] + U^2(1-\mu_j^2)/(4E_j\bar{E}_j)\right|} \tag{10}$$

where α–$\alpha' = l$–λ or ρ–r.

As a specific feature of this result, we can mention the fact that, for the gapless mode $j \equiv j^* = 2(\mathcal{N}+1)/3$ (if $\mathcal{N}+1$ is divisible by 3), we have $\mu_{j^*} = 1$. Hence, for $j = j^*$,

$$T^{(j^*)}_{\alpha-\alpha'} = \frac{\sin\theta\sin\bar{\theta}}{\sin^2[(\theta+\bar{\theta})/2]}. \tag{11}$$

It is important to note that, as shown in Ref. [17], relation (11) defines the transmission coefficient for an r–l interface for any j. In the next section, we show that the same is true for α–$\alpha' = \lambda$–ρ.

2.2 λ–ρ and r–l interfaces As mentioned above, the electron transmission through the r–l interface between zero and nonzero potentials has already been studied with the use of the matching technique [17] and the Lippman–Schwinger equation [18]. Therefore, we consider the case of λ–ρ interface shown in Fig. 1c. Recall that within the λ–ρ and r–l pairs, which alternately form parallel chains of A–B sites across the ribbon, the phase of the wave function differs by θ.

Substituting Eq. (3) into the second and third equation of Eq. (2) for $n = 0$, we obtain

$$E\psi^{\mathrm{L}}_{m,0,\lambda} = -\psi^{\mathrm{L}}_{m,0,l} - \psi^{\mathrm{L}}_{m-1,0,l} - \psi^{\mathrm{R}}_{m,0,\rho},$$
$$\bar{E}\psi^{\mathrm{R}}_{m,0,\rho} = -\psi^{\mathrm{R}}_{m,0,r} - \psi^{\mathrm{L}}_{m-1,0,r} - \psi^{\mathrm{L}}_{m,0,\lambda}. \quad (12)$$

With $t^{(j)}$ found from this pair of equations, the same way of calculations leads us to the following expression of the transmission coefficient:

$$T^{(j)}_{\alpha-\alpha'} = \frac{\sin\theta \sin\bar{\theta}}{\sin^2[(\theta+\bar{\theta})/2]}, \quad (13)$$

which is valid for $\alpha-\alpha' = \lambda-\rho$. The same relation was found in [17] for $\alpha-\alpha' = r-l$. It coincides with the preceding result (10) only for $j = j^*$.

The case $j = j^*$ is special because the phase difference θ_{j^*} is independent of the aGR width,

$$2\cos^2\theta_{j^*} = 1 \pm \cos\left(\frac{\sqrt{3}k}{2}\right). \quad (14)$$

In the long-wave limit, $\cos^2\theta_{j^*} \approx 1$ for the "+" branch and $\cos^2\theta_{j^*} \approx 3k^2/16$ for the "−" branch. For small energies with $\sqrt{3}k \ll \pi$, $|\theta_{j^*}| \approx \pi/2$ is associated with Berry's phase [20].

Furthermore, except the trivial case $U = 0$, the mode transmission coefficient is equal to 1, i.e., there is no backscattering only for $k = \bar{k}$, when the gate potential equalizes $\bar{E}_j$ with E_j. In other words, this happens only when the electron state in the valence band has the same energy and wave vector as the incident electron. Hence, the phase θ_j just changes its sign, $\theta_j(k) = -\bar{\theta}_j(\bar{k} = k)$. It is thus not surprising that the interband transmission from the conduction to valence band, or *vice versa*, which essentially involves the same states has the probability 1.

Expression (13) has the following important property: its form coincides with the form of the corresponding expression for tight-binding chains. It is rather easy to obtain the transmission coefficient for the step-like structure consisting of a half-infinite chain with a wave vector k connected to a half-infinite chain with a wave vector $\bar{k}$, $k, \bar{k} \geq 0$. Proceeding in the same way as above, we derive a well-known formula

$$T(E) = \frac{\sin k \sin\bar{k}}{\sin^2[(k+\bar{k})/2]} \xrightarrow[k,\bar{k}\to 0]{} \frac{4k\bar{k}}{(k+\bar{k})^2}, \quad (15)$$

where $E = -2\cos k$, $\bar{E} = E - U = -2\cos\bar{k}$, and the limit of small wave vectors corresponds to the effective mass approximation. Thus, the transmission coefficient (13) for the r–l interface represented in terms of phase quantities has exactly the same form as the coefficient of transmission through two tight-binding chains with different site energies, represented in terms of wave vectors.

2.3 aGRs of arbitrary width Relations (10) and (13) are valid for any $\mathcal{N}$. If $j^* = 2(\mathcal{N}+1)/3$ is an arbitrary integer, then μ_{j^*}=1 implies that the metallic mode transmission is the same for any position of the potential step. Hence $T^{(j^*)}_{r-l} = T^{(j^*)}_{l-\lambda} = T^{(j^*)}_{\lambda-\rho} = T^{(j^*)}_{\rho-r}$, and for all other modes, $T^{(j\neq j^*)}_{rl}$ $= T^{(j\neq j^*)}_{\lambda-\rho} \neq T^{(j\neq j^*)}_{l-\lambda} = T^{(j\neq j^*)}_{\rho-r}$. As a consequence, the appearance of $T(E_{\mathrm{F}}, U)$ (where E_{F} is the Fermi energy) in armchair graphene ribbons strongly depends on the location of the change in potential. This statement is illustrated in Sections 2.4 and 2.5.

The cause of the indicated transmission dependence is that θ_j determines the phase difference between the A and B sites with identical transverse coordinate m or $m - 1/2$. Therefore, if the nearest neighbors on both sides of the interface belong to the same A–B pair, then scattering can be described in terms of the change $\theta_j \to \bar{\theta}_j$. This is obviously impossible if the interface divides the sites with different transverse coordinates.

In view of the spectrum symmetry, we have

$$T^{(j)}(-|E|, U) = T^{(j)}(|E|, -U).$$

Obviously, $T^{(j)}(E, U = 0) = 1$. The nonzero values of U mimic the effect of gate voltage applied to the right half of the ribbon at different values of the Fermi energy $E = E_{\mathrm{F}}$. This also concerns zigzag GRs. According to the Landauer approach, formulas (10) and (13) determine the dependence of the Ohmic current on the external parameters E_{F} and U in the related electron-transport experiments.

2.4 Narrow aGRs (2aGRs) As an example, we consider one- and two-mode transmission in the most narrow armchair graphene ribbon with gapless spectrum ($\mathcal{N} = 2$, $j^* = 2$). The second mode ($|E_2(k)| \leq 2$) has a linear dispersion if $|E_2(k)| \ll 1$. This dispersion dominates the energy interval $|E = E_2(k)| < \sqrt{3}-1$, where only the single-mode transmission is possible. The transmission coefficient is close (but not equal) to one if the potential step varies within the same energy interval as illustrated by the top row in Fig. 2. As follows from Eq. (11), in this energy interval, the transmission coefficients for the λ–ρ and l–λ interfaces are identical. In contrast, for $j = 1$, single-mode transmission for both interfaces (third and bottom rows in the same figure) is zero within the energy interval $|E = E_1(k)| < \sqrt{3} - 1$, which manifests the prohibition of intermode transmission due to the mode orthogonality. For the same reason, the functions $T(E_{\mathrm{F}}, U)$ shown in the second and fourth rows have a jumplike shape associated with switching (on/off) of one of two modes. These features are similar for both interfaces.

At the same time, pronounced differences between the behavior of the transmission coefficient for the λ–ρ and l–λ interfaces can be seen when $U > 0$ and $E_{\mathrm{F}} > \sqrt{3} - 1$. As U increases, transmission is significantly suppressed in the latter case as compared with the former case. This trend is preserved for larger $\mathcal{N}$.

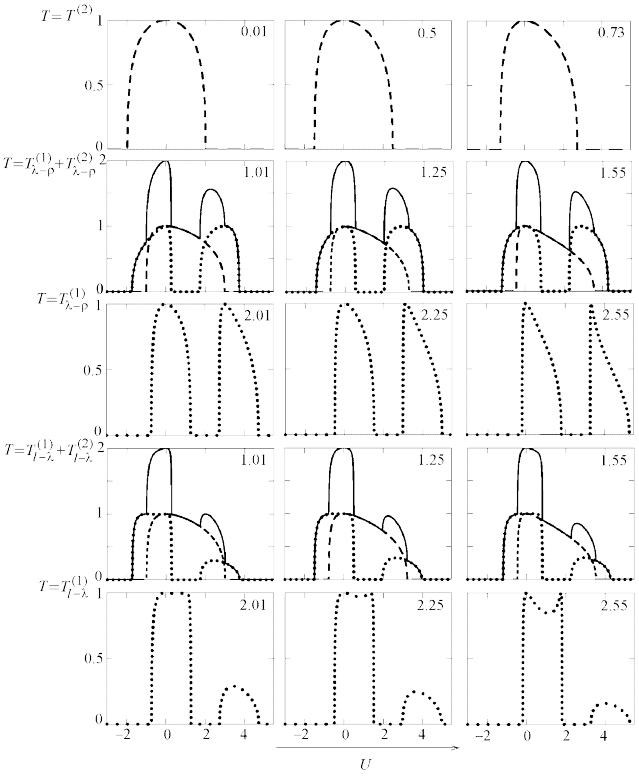

Figure 2 Through λ–ρ (three upper rows) and l–λ (two lower rows) step transmission in 2aGR as a function of the right-gate potential, $\sum_j T^{(j)}_{\alpha-\alpha'} \equiv T$: $T^{(1)}_{\alpha-\alpha'}(U)$ (dotted curves), $T^{(2)}_{\alpha-\alpha'}(U)$ (dashed curves), $T^{(1)}_{\alpha-\alpha'}(U) + T^{(2)}_{\alpha-\alpha'}(U)$ (solid curves). The panels are labeled by the values of incident-electron energy set equal to E_F. The top row represents a single-mode transmission when the first conduction band is partly filled ($0 \le E_F < \sqrt{3}-1$). In this energy interval, the transmission coefficient is identical for both types of interfaces: $T^{(2)}_{\lambda-\rho} = T^{(2)}_{l-\lambda} \equiv T^{(2)}$. The second and forth rows correspond to the two-mode transmission when both conduction bands are partly filled ($\sqrt{3}-1 \le E_F < 2$). The bottom and third rows correspond to the single-mode transmission when the first conduction band is completely filled but the second band is filled only partly ($2 < E_F < \sqrt{3}+1$); E_F and U are in the units of β.

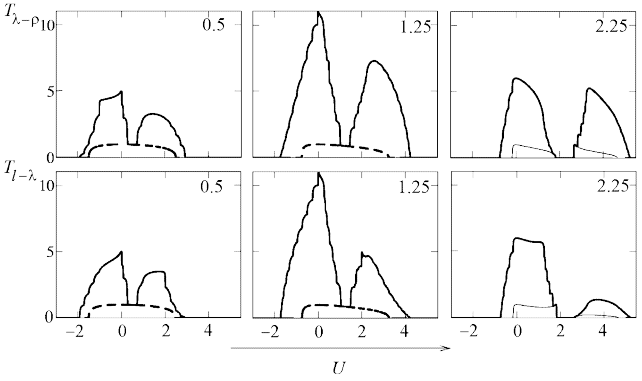

Figure 3 Through λ–ρ (upper row) and l–λ (lower row) step transmission in aGR with $\mathcal{N} = 11$ as a function of the right-gate potential, $\sum_j T^{(j)}_{\alpha-\alpha'} \equiv T_{\alpha-\alpha'}$ (solid curves). The function $T^{(j^*=8)}_{\alpha-\alpha'}(U)$ is plotted with the dashed lines (the first and second columns), and the function $T^{(j^*-2=6)}_{\alpha-\alpha'}(U)$ is plotted with the thin solid lines (the third column). The panels are labeled by the values of incident-electron energy set equal to E_F. The first column represents the five-mode transmission, i.e., for $E_F = 0.5$, the bands $j = 6, \ldots, 10$ are open for charge carriers. The second column corresponds to the eleven-mode transmission when all the bands are open. The third column corresponds to the six-mode transmission when the bands $j = 1, \ldots, 6$ are open. E_F and U are in the units of β.

Summarizing the inherent properties of polyperylene as a molecular wire, we conclude that it must exhibit the conductance $\approx 2e^2/\hbar$ weakly depending on the changes in the Fermi energy and gate potential if $|E_F|, |U| < \sqrt{3}-1$ ($\sim$2 eV). For $E_F < \sqrt{3}-1$, the single-mode transmission is identical for both types of interfaces. For larger E_F, the difference between the transmission coefficients for λ–ρ and l–λ interfaces is more pronounced for positive U, and the same is true for aGR of arbitrary width. The gap of zero conductance for large $|E_F|$ decreases as $\mathcal{N}$ increases.

It is important to note, that the transmission coefficient $T^{(j)}_{\alpha-\alpha'}$ depends on $\mathcal{N}$ only via the quantity μ_j. Therefore, independently of the aGR width, the behavior of $T^{(j)}_{\alpha-\alpha'}$ remains similar for equal μ_j, or, which is the same, for the modes and $\mathcal{N}$ having equal relation $j/(\mathcal{N}+1)$. The most important example is the case of $j = j^*$ for metallic aGR: independently of the aGR width, the dependence $T^{(j^*)}_{\alpha-\alpha'}(E, U)$ remains the same, namely, its behavior is represented by the dashed curves in Fig. 2. The dotted curves in the same figure represent not only $T^{(1)}_{\alpha-\alpha'}$ for $\mathcal{N} = 2$, but also $T^{(2)}_{\alpha-\alpha'}$ for $\mathcal{N} = 5$, $T^{(3)}_{\alpha-\alpha'}$ for $\mathcal{N} = 8$, and, generally speaking, for all pairs of values of j and $\mathcal{N}$ which satisfy $j/(\mathcal{N}+1) = 1/3$. Thus, the presented curves show the energy dependence of the transmission coefficient for some modes for the ribbons wider than $\mathcal{N} = 2$. To show the behavior of the sum of $T^{(j)}_{\alpha-\alpha'}(E, U)$ for wider ribbons, in the next section, we consider the case $\mathcal{N} = 11$.

2.5 Wider aGRs ($\mathcal{N} = 11$)

In Fig. 3, we represent the through step transmission $T = \sum_j T^{(j)}_{\alpha-\alpha'}$ as a function of the right-gate potential in aGR with $\mathcal{N} = 11$. The width is chosen to provide the possibility to compare the obtained results with the previously reported dependences for $T^{j^*-1}_{r-l}$, $T^{j^*}_{r-l}$, and $T^{j^*+1}_{r-l}$ obtained with the help of the Green's functions method [18]. Here, we pay the main attention to the overall transmission coefficient $\sum_j T^{(j)}_{\alpha-\alpha'}$ and to the difference in the functions for the λ–ρ and l–λ interfaces. Depending on the values of incident-electron energy, all modes or only several modes contribute to the transmission. The dispersion relation (4) immediately gives the following criterion for the band opening: the jth band is open if $|1-\mu_j| \le E_F \le 1+\mu_j$. Then, for $E_F = 0.5$ we obtain the five-mode transmission (first column in Fig. 3), while for $E_F = 1.25$ all the modes of aGR with $\mathcal{N} = 11$ are conducting.

As it was the case for 2aGR, for wider aGRs the transmission coefficients for the λ–ρ and l–λ interfaces are substantially different for $U > 0$ and large E_F, see third column in Fig. 3. As U increases, the transmission through l–λ step is

much lower as compared to the case of the λ–ρ interface. This feature of the transmission in aGRs can be used to identify the type of interfaces in the experiments aimed at measuring the conductivity of aGR-based electronic devices.

3 Transmission in 1zGR Polyacene (width 2.84 Å), as a molecular wire, provides two pathways for an excess electron, and the same is true for polyperylene (width 4.26 Å). Furthermore, the π-electron spectrum of both polymers is semimetallic. Therefore, one can expect a similar behavior of through-step transmission near the neutrality point. We now show that this expectation is not justified. In fact, the single-mode through-step transmissions in 2aGR and 1zGR are rather different as long as E_F is not far away from the neutrality point.

In 1zGR, the appearance of two modes is connected with the parity of eigenstates: symmetric and antisymmetric, $j = s, a$. The energies of these states are partly overlapping [21],

$$2E_{s(a)} = \mathrm{sign}[E_{s(a)}]\sqrt{1+16\cos^2(k/2)} - (+)1,\ \varepsilon_m{=}0,$$
$$2\bar{E}_{s(a)} = \mathrm{sign}[\bar{E}_{s(a)}]\sqrt{1+16\cos^2(\bar{k}/2)} - (+)1,\ \varepsilon_m{=}U. \tag{16}$$

The wave function amplitudes at the physically equivalent atoms l, r and λ, ρ, have the same or opposite signs for symmetric or antisymmetric states, respectively. The pairwise sums and differences of these amplitudes, $\psi^{s(a)}_{m,lr} = \psi^{s(a)}_{m,l} + (-)\,\psi^{s(a)}_{m,r}$, $\psi^{s(a)}_{m,\lambda\rho} = \psi^{s(a)}_{m,\lambda} + (-)\,\psi^{s(a)}_{m,\rho}$ obey the following equations:

$$(E-\varepsilon_m)\,\psi^{s(a)}_{m,lr} = -\psi^{s,(a)}_{m,\lambda\rho} - \psi^{s(a)}_{m+1,\lambda\rho},$$
$$[E-\varepsilon_m+(-)\,1]\,\psi^{s(a)}_{m,\lambda\rho} = -\psi^{s(a)}_{m,lr} - \psi^{s(a)}_{m-1,lr}, \tag{17}$$

where $\varepsilon_m = 0$ or U.

The expression for eigenstates of zigzag graphene ribbons with zero site energies was obtained in Ref. [12]. In the case in focus, $N = 1$, functions satisfying Eq. (17) with $\varepsilon_m = 0$ can be represented as

$$\psi^{s(a)}_{m,lr} = +(-)\sqrt{\frac{E_{s(a)}+(-)\,1}{E_{s(a)}}}\,e^{ikm},$$
$$\psi^{s(a)}_{m,\lambda\rho} = -(+)\,\mathrm{sign}[E_{s(a)}]\,e^{ik(m-1/2)}. \tag{18}$$

At this point, it is worth emphasizing that 2aGR also has axial symmetry and, consequently, the wave functions at the pairs of sites $1, n, l(r)$, $2, n, l(r)$ and $1, n, \lambda(\rho)$, $3, n, \lambda(\rho)$ are either identical or have different signs. However, unlike the case of 1zGR, the equations for the "±" combinations $\psi^{(j)}_{m,n,l(\lambda)} \pm \psi^{(j)}_{m,n,r(\rho)}$ turn out to be coupled because of the phase difference between r and l, and λ and ρ sites. As a result, the selection rule in aGR corresponds to different modes, whereas in 1zGR, it corresponds to different parities of the states. This principal distinction concerns armchair and zigzag graphene ribbons of any width. It is also the cause of substantial distinctions in the electron transport properties along armchair and zigzag pathways.

As in the previous section, we can construct the solution to Eq. (17) with $\varepsilon_{m<1} = 0$ and $\varepsilon_{m\geq 1} = U$ in the form of Eq. (3), where $j \to s(a)$, $\alpha = lr, \lambda\rho$, and the index $n = 1$ is omitted, see Fig. 1. The usage of Eqs. (3) and (18) thus modified in Eq. (17) yields an expression for $t^{s(a)}$ and, hence, for the respective transmission coefficient

$$T^{s(a)} = \frac{4\sin k^{s(a)}\sin \bar{k}^{s(a)}}{F_1 - F_2}, \tag{19}$$

$$F_1 = E_{s(a)}\left|\bar{E}_{s(a)}+(-)1\right| + \left|\bar{E}_{s(a)}\right|\left[E_{s(a)}+(-)1\right],$$
$$F_2 = 8\,\mathrm{sign}[\bar{E}]\cos\frac{k^{s(a)}}{2}\cos\frac{\bar{k}^{s(a)}}{2}\cos\frac{k^{s(a)}+\bar{k}^{s(a)}}{2}. \tag{20}$$

As before, we restrict ourselves to positive energies of incident electrons. It is also worth noting that the superscript of the wave vector corresponds to the dispersion relation used in calculations, whereas the overbar refers to 1zGR with $\varepsilon_m = U$.

The π-electron spectrum of polyacene is symmetric with respect to the site energy. According to Eq. (16), the bands of symmetric and antisymmetric states alternate. If, e.g., the energy of incident electron lies within the lowest conduction band (symmetric states), then the step potential $U = E_F$ makes the highest valence band open for electron transmission (antisymmetric states). However, this transmission is forbidden by the selection rule.

Thus, despite its semimetallic spectrum, polyacene can behave as a semiconducting polymer, like, e.g., polyparaphenylene. It is the case where $|E_F| < 1$, as illustrated in Fig. 4, the top row, where the transmission coefficient (i.e., the Ohmic conductance) is equal to zero within the interval $0 < U < 1$ (~2.5–3 eV). This is in a striking contrast with the transmission in 2aGR; see Fig. 2. However, for larger $|E_F|$, as illustrated in Figs. 2 and 4 by all but the top panel rows, the behavior of the transmission coefficient has many common features. Moreover, for $E_F > 2$, the transmission coefficient of 2aGR with l–λ interface is quite similar to the transmission coefficient of 1zGR.

4 Conclusions To conclude, we have found the transmission coefficients for armchair GRs of any width with different interfaces between the regions with zero and nonzero site energies. For GRs with zigzag-shaped edges, we considered the case of transmission for $N = 1$, i.e., for polyacene. The obtained explicit expressions allow us to compare the transmission coefficients for two types of graphene nanoribbons: 2aGR and 1zGR. One of numerous implications of this comparison is that a segment of 2aGR with a side stub of 1zGR can be regarded as a three-terminal multifunctional electronic device with easily adjustable characteristics.

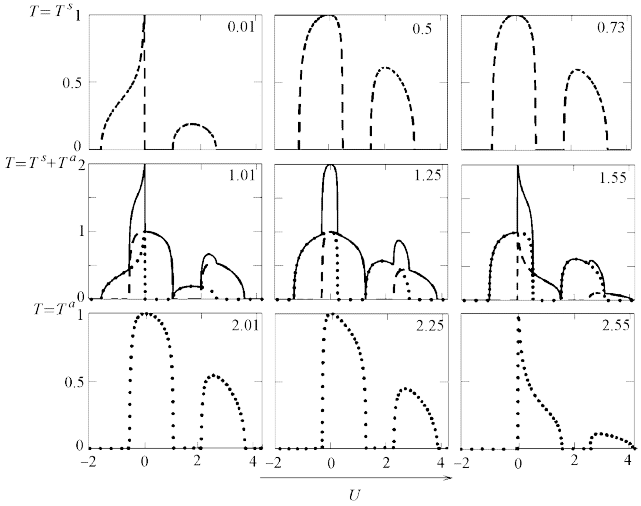

Figure 4 Through step transmission in 1zGR as a function of the right-gate potential, $T = T^s + T^a$: $T^s(U)$ (dashed curves), $T^a(U)$ (dotted curves), $T^s(U) + T^a(U)$ (solid curves). The panels are labeled by values of the incident-electron energy set equal to E_F. The top row represents a single-mode transmission of symmetric wave-states when the first conduction band is partly filled ($0 \leq E_F < 1$), the middle row reflects the two-mode transmission when both conduction bands are partly filled ($1 \leq E_F < 1.56$), the bottom row corresponds to single-mode transmission of antisymmetric wave-states when the first conduction band is completely filled but the second is filled only partly ($1.56 < E_F < 2.56$).

Acknowledgement This work was partly supported by Special Program of Division of Physics and Astronomy of NASU.

References

[1] X. L. Li, X. R. Wang, I. Zhang, S. W. Lee, and H. J. Dai, Science **319**, 1229 (2008).
[2] D. V. Kosynkin, A. L. Higginbotham, A. Sinitskii, J. R. Lomeda, A. Dimiev, B. K. Price, and J. M. Tour, Nature **458**, 872 (2009).
[3] X. L. Jiao, X. R. Wang, G. Diankov, H. L. Wang, and H. J. Dai, Nature Nanotechnol. **5**, 321 (2010).
[4] C. Tao, L. Jiao, O. V. Yazyev, Y.-Ch. Chen, J. Feng, X. Zhang, R. B. Capaz, J. M. Tour, A. Zettl, S. G. Louie, H. Dai, and M. F. Crommie, Nature Phys. **7**, 616 (2011).
[5] J. Baringhaus, M. Ruan, F. Edler, A. Tejeda, M. Sicot, A. Taleb-Ibrahimi, A.-P. Li, Z. Jiang, E. H. Conrad, C, Berger, C. Tegenkamp, and W. A. de Heer, Nature **506**, 349 (2014).
[6] T. Ando, T. Nakanishi, and R. Saito, J. Phys. Soc. Jpn. **67**, 2857 (1998).
[7] N. M. R. Peres, A. H. Castro Neto, and F. Guinea, Phys. Rev. B **73**, 195411 (2006).
[8] J. Tworzydlo, B. Trauzettel, M. Titov, A. Rycerz, and C. W. J. Beenakker, Phys. Rev. Lett. **96**, 246802 (2006).
[9] V. V. Cheianov and V. I. Fal'ko, Phys. Rev. B **74**, 041403(R) (2006).
[10] K. Wakabayashi and M. Sigrist, Phys. Rev. Lett. **84**, 3390 (2000).
[11] L. Malysheva and A. Onipko, Phys. Rev. Lett. **100**, 186806 (2008).
[12] A. Onipko, Phys. Rev. B **78**, 245412 (2008).
[13] Y. Hancock, A. Uppstu, K. Saloriutta, A. Harju, and M. J. Puska, Phys. Rev. B **81**, 245402 (2010).
[14] J. Ruseckas, G. Juzeliünas, and I. V. Zozoulenko, Phys. Rev. B **83**, 035403 (2011).
[15] K. Wakabayashi, K. Sasaki, T. Nakanishi, and T. Enoki, Sci. Technol. Adv. Mater. **11**, 054504 (2010).
[16] L. Malysheva, Phys. Status Solidi B **251**(5), 1028–1033 (2014).
[17] Yu. Klymenko, L. Malysheva, and A. Onipko, Phys. Status Solidi B **245**, 2181 (2008).
[18] L. Malysheva, E. Petrenko, and A. Onipko, Phys. Status Solidi B **246**, 2405 (2009).
[19] Yu. Klymenko and O. Shevtsov, Eur. Phys. J. B **69**, 383 (2009); Eur. Phys. J. B **72**, 203 (2009).
[20] M. V. Berry, Proc. R. Soc. Lond. A **392**, 45 (1984).
[21] S. Kivelson and O. L. Chapman, Phys. Rev. B **28**, 7236 (1983).